Arabian Journal of Chemistry 16 (2023) 105349

Contents lists available at ScienceDirect

Arabian Journal of Chemistry

journal homepage: www.sciencedirect.com

Original article

Facile synthesis of palladium nanoparticles/polypyrrole-carbon black/Bi_2O_3 ternary nanocomposite for efficient photocatalytic degradation of colorless and colored pollutants under visible light

M. Faisal [a,b], Jahir Ahmed [a,b], Jari S. Algethami [a,b], Mabkhoot Alsaiari [a,c], Farid A. Harraz [a,c,*]

[a] Promising Centre for Sensors and Electronic Devices (PCSED), Advanced Materials and Nano-Research Centre, Najran University, Najran 11001, Saudi Arabia
[b] Department of Chemistry, Faculty of Science and Arts, Najran University, Najran 11001, Saudi Arabia
[c] Department of Chemistry, Faculty of Science and Arts at Sharurah, Najran University, Sharurah 68342, Saudi Arabia

ARTICLE INFO

Article history:
Received 7 August 2023
Accepted 8 October 2023
Available online 11 October 2023

Keywords:
Bi_2O_3
Ternary photocatalyst
Pd NPs
Ultrasonication
Photoreduction
Imidacloprid

ABSTRACT

In present report, an efficient, reliable ternary photocatalyst based on Bi_2O_3 nanostructure accompanied by polypyrrole doped carbon black (PPC) and palladium nanoparticles (Pd NPs) was created employing simple ultra-sonication and photo-reduction methodologies for treatment of contaminated water. XRD studies confirmed the tetragonal phase of β-Bi_2O_3 while elemental composition and nanocomposite development amongst Pd NPs, PPC and Bi_2O_3 has been confirmed by XPS and FTIR investigations. TEM studies revealed the presence of Pd NPs of 5–15 nm, stacked layers of dense beads of PPC along with irregular ball like particles of Bi_2O_3 grown in high density in designed ternary photocatalyst. Newly developed Pd@PPC/Bi_2O_3 photocatalytic framework was found to be highly effective when employed on colorless insecticide imidacloprid (IMD) and methylene blue (MB) dye under visible light. Newly fabricated Pd@PPC/Bi_2O_3 photocatalyst showed excellent removing skills with 93.60 % elimination of IMD just in 30 min representing 276 % more effectual than pristine Bi_2O_3. Furthermore, Pd@PPC/Bi_2O_3 nanostructure was found to be stable and exceptionally active towards MB, with a total dye elimination achieved within 12 min. Enhanced performance of the ternary photocatalyst was attributed to increased surface area, enhanced charge carrier transfer with better separation behavior.

1. Introduction

Continuous introduction of untreated hazardous metabolites and dangerous chemicals into the nearby surrounding developed severe disorders and health problems between different existing flora and fauna (Alam et al., 2017; Faisal et al., 2011; Faisal et al., 2011; Farah et al., 2004). Hence, for such panic situation, specifically for water pollution issue, a precise, competent, and cost-effective treatment approach is urgently required. At present, the best available treatment methodology is semiconductor mediated photocatalytic treatment of noxious pollutants (Masula et al., 2023; Gade et al., 2018; Masula et al., 2022; Gade et al., 2022; Rao et al., 2021).

Nowadays, bismuth oxide: Bi_2O_3 was proven to be extremely potent semiconducting material due to suitable band gap (Shimizugawa et al., 1997), high refractive index, promising photoconductivity/photoluminescence, and dielectric permittivity (Shimanoe et al., 1998). Bi_2O_3 has been utilized in various sectors for different applications like in superconductor ceramic glass (Pan and Ghosh, 2000), sensor optical coating (Leontie et al., 2002), electroreduction (Pérez et al., 2005) and in electrolyte (Sarat et al., 2006). Bi_2O_3 exhibited six polymorphic phase denoted by α: monoclinic, β: tetragonal, γ: cubic (bcc), δ: cubic (fcc), ε: orthorhombic and ω: Bi_2O_3 (triclinic) (Yilmaz et al., 2011; Mehring, 2007; Drache et al., 2007). Among various phases, α and δ-Bi_2O_3 phases are recognized to be quite stable while other phases are high-temperature metastable (Leontie et al., 2002). In addition, this thermodynamically α-Bi_2O_3 was found to be most stable phase in the range of 25––730 ^{0}C (Ho et al., 2013; Vila et al., 2012). At 730 ^{0}C, α-Bi_2O_3 transforms into δ-Bi_2O_3 with stability up to 825 °C (Lin and Wei, 2011). Among these various

* Corresponding author.
E-mail address: faharraz@nu.edu.sa (F.A. Harraz).
Peer review under responsibility of King Saud University.

Production and hosting by Elsevier

https://doi.org/10.1016/j.arabjc.2023.105349
1878-5352/

polymorphic forms of Bi_2O_3, α- and β-Bi_2O_3 has been exploited effectually under visible light (Ho et al., 2013). Also, some researchers observed that β-phase showed better photocatalytic performance than α- Bi_2O_3. Therefore, some devoted and focused efforts are perquisite for β-Bi_2O_3 to further improved its performance.

In recent times, it has been very well established that hybrid photocatalyst in conjugation with polymeric metabolites found to be extremely efficacious with encouraging photocatalytic results (Li et al., 2017; Nsib et al., 2015; Riaz et al., 2015; Luo et al., 2017; Li et al., 2017). Allied polymeric organization supposed to have boosting and multifunctional outcomes like: (i) Polymeric structures proven to be productive photosensitizer due to flexible wide-range visible light captivation skills. (ii) Delivers hassle-free channels for uninterrupted transferal of charge with better separation skills. (iii) Offers impeccable heterojunction with semiconducting nanostructures for constant interfacial charge transference (Li et al., 2017; Nsib et al., 2015; Riaz et al., 2015; Luo et al., 2017; Li et al., 2017). Conducting organic polymers which includes polypyrrole, polythiophene and polyaniline recognized to be extremely feasible for the creation of promising hybrid photocatalytic framework with semiconducting metabolites. Among these, polypyrrole (PP) noticed to be quite consistent with sufficient stability and good conductivity. PP has very simple and straight forward synthesis procedure (Ansari, 2006). PP possessed band gap in the range of 2.2–2.4 eV works smoothly under visible light (Oh et al., 2005). This productive polymer has been comprehensively utilized in numerous sectors for wide range of applications like in elimination of cancerous tomours / tissues (Jeon et al., 2014; Zha et al., 2013), fuel cells / catalysis (Yao et al., 2014), super capacitor electrodes (Shi et al., 2014; Huang et al., 2015) and actuators (Naficy et al., 2013), etc. It is pertinent to mention here that composites photocatalytic structure among PP with non-metallic metabolites like carbon proven to be quite productive with boosted performance (Marschall and Wang, 2014).

Very recently, numerous hybrid photocatalyst of Bi_2O_3 with precious metals have been exploited in environmental management processes and these hybrid photocatalysts found to be quite competent and effective with excellent photocatalytic performance (Zhong et al., 2014; Parvathi et al., 2021; Anandan et al., 2010; Li et al., 2014). Efficacious linkage among noble metal (dielectric confined electronic phase) and semiconductor (quantum confined electronic phase) offered framework with outstanding optoelectronic properties (Daniel and Astruc, 2004; Larkin et al., 2004; Figuerola et al., 2010). Furthermore, LSPR effect between involved noble metal and semiconductor increases the absorption skills of developed framework with favorable exciton dynamic (Shaviv et al., 2011; Sagarzazu et al., 2013). Hybrid electronic states of involved moieties provides swift /effectual charge transference at metal–semiconductor boundary (Haldar et al., 2012; Jakob et al., 2003; Costi et al., 2009) along with augmentation in visible light captivation, supposed to highly fruitful for efficacious and favorable photocatalytic reactions (Elmalem et al., 2008; Costi et al., 2008).

Owing to LSPR effect, the local electromagnetic field significantly boosts up the surface of metallic NPs. Theoretically, more is the electromagnetic intensity more effective is the photogenerated electron–hole pairs separation as S. Lv and coworkers designed a Ag/AgX nanocomposite photocatalyst for CO_2 photoreduction and observed that production of CH_4 in 1 h was improved to 28.7 times (Lv et al., 2022). The enhancement in photocatalytic activity could be attributed to increased separation velocity of electron–hole pairs and the close-range dipole–dipole resonance at the interface between the semiconductor and metal due to the enhanced local electromagnetic field. It has been noticed that the excited electrons mainly located in the shallow position below the surface of semiconductor, allowing an extremely short diffusion distance to the surface. Hence, due to local electromagnetic field, electron–hole pairs could be rapidly generated near the semiconductor surface and promptly migrate to the surface to have oxidation/reduction reactions (Lv et al., 2022).

Considering the above promising special features of conducting polymer/ semiconducting photocatalyst as well as encouraging outcomes by noble metal/semiconductor combination, we focused our research on the designing of a trio photocatalysts based on noble metal, conducting polymer and a semiconducting material i.e. a photocatalyst possessed Pd NPs, polypyrrole doped carbon black (PPC) and Bi_2O_3. Fabricated Pd@PPC/Bi_2O_3 photocatalyst has been successfully utilized for the management of colorless insecticide imidacloprid (IMD) and on methylene blue (MB) dye. Main aim of current research is to work out a strategy to enhance performance of Bi_2O_3. As per previous literature and to best of author's knowledge this is the first study regarding the deployment of newly created Pd@PPC/Bi_2O_3 nanostructures as photocatalyst for environmental cleansing issue.

2. Experimental

2.1. Materials and methods

Polypyrrole doped carbon black, Bismuth (III) oxide: Bi_2O_3 nanopowder, palladium (II) chloride methylene blue, isopropanol, nafion, CH_3OH and C_2H_5OH were procured from Sigma Aldrich.

2.2. Preparation of PPC/Bi_2O_3 and Pd@PPC/Bi_2O_3

10 %PPC/Bi_2O_3 nanocomposites represented as PPC/Bi_2O_3 were came into existence by applying ultra-sonication method. Briefly, 1 g of Bi_2O_3 nanopowder was poured in 100 ml of DI water along with 0.1 g of PPC and mixed (constant stirring) for about 20 min. Obtained solution was then ultra-sonicated for about 40 min. Attained mixture then washed appropriately with ethanol and DI water, dried in oven at 65 °C for 24 h to attained PPC/Bi_2O_3 nanostructures. Subsequently, for the fabrication of prerequisite 1 % Pd@10 %PPC/Bi_2O_3 trio photocatalytic framework, photoreduction technique as reported previously was employed (Faisal et al., 2022). Desired weight of palladium (II) chloride (solid) has been taken (contained 1 wt% of Pd), carefully mixed in 0.5 gms of 10 % PPC/Bi_2O_3 suspension and irradiated by Hg lamp (Osram) having 2.0 $mWcm^{-2}$ intensity for 14 h. After completion of irradiation process, mixture was then centrifuged to separate the required material. Later, the acquired material was then washed with ethanol/DI water, dried at 65 °C/24 h to obtain 1 % Pd@10 % PPC/Bi_2O_3 named as Pd@PPC/Bi_2O_3 throughout the entire manuscript.

The formation mechanism of the synthesized Pd@PPC/Bi_2O_3 nanocomposite may involve several steps, including the preparation of PPC/Bi_2O_3 composite and subsequent deposition of Pd NPs onto the composite. A general overview of the formation mechanism includes firstly the ultrasonication step to disperse PPC and Bi_2O_3 in DI water. During this process, the particles may be broken down into smaller sizes, ensuring good dispersion and intimate contact between the components. Then, in the next step during the photoreduction process, the reduction of Pd ions occurred upon exposure to light to produce Pd NPs deposited onto the surface of the PPC/Bi_2O_3 composite. The photoreduction process starts with the absorption of photons by the composite material, particularly the semiconductor Bi_2O_3, leading to electrons excitation from the valence band to the conduction band, creating electron-hole pairs. The excited electrons can then transfer to Pd ions, reducing them in the solution, leading finally to the deposition of Pd NPs. Such elec-

tron transfer process may be facilitated by PPC, which may act as an electron donor or mediator. The deposited Pd NPs may interact with the surface of the PPC/Bi_2O_3 composite via either chemical bonding or physical adsorption, further enhancing their stability and catalytic activity.

2.3. Materials characterization

XRD measurement of prepared samples was successfully accomplished on AXS D4 Endeavour model of Bruker diffractometer utilizing Cu K$\alpha_{1/2}$, $\lambda\alpha_1$ = 154.060 pm and $\lambda\alpha 2$ = 154.439 pm radiation. Surface morphology and other associated features were comprehensively analyzed on 5 kV -field emission scanning electron microscope (JEOL-6300F) and on JEOL JEM-2100F-UHR model of transmission electron microscope at 200 kV, fitted with 1 k CCD camera and Gatan energy filter: GIF 2001. FTIR spectra of fabricated nanostructures has been recorded on Spectrum 100 model of Perkin Elmer spectrometer (in range 400–4000 cm^{-1}) under KBr pellet mode. XPS investigations were conducted on 200R: VGESCALAB spectrometer fitted with hemispherical electron analyzer applying MgKα monochromatic X-ray source (hν = 1253.6 e V). Prior to analysis each sample was appropriately degassed. PL spectra of each sample was successfully acquired on Hitachi fluorescence (F-7000) spectrophotometer at 325 nm excitation wavelength. Surface area was examined on NOVA 4200 model of Quantachrome analyzer at 77 K. Each tested sample has been degassed for 12 h at 200 ^{0}C. Diffuse reflectance spectra for each sample in the range 800 nm to 200 nm has been recorded on UV–Vis −3600: Shimadzu spectrophotometer. Acquired values of % R were then utilized in Kubelka-Munk function *versus* Energy i.e. $[F(R)\,E]^2$ *versus* E to evaluate the bandgap (E_g) for various fabricated samples applying the below mentioned equation:

$$F(R)E^2 = \left(\frac{(1-R)^2}{2R} \times h\upsilon\right)^2$$

Where F(R) stands for Kubelka–Munk function, R is the reflectance, E is the incident photon energy.

2.4. Photocatalytic experiments

Different created photocatalyst were tested for photocatalytic performance evaluation taking imidacloprid (IMD) and methylene blue (MB) dye as aim analytes. All photocatalytic trials were conducted in photo-reaction assembly (150 ml) of quartz glass. For illumination process, visible light lamp (250 W) procured from Lelesil Mumbai (India) was utilized, the spectra of this lamp is provided in Supplementary Information. Photo-reactor have well designed water circulation channels to control the excess heat generated and continuous air was supplied to the reaction solution during the entire reaction process. Typically, for individual photocatalytic reaction, 100 mg of fabricated photocatalyst was mixed with 100 ml of IMD (concentration 20 ppm) in reaction assembly. Adsorption factor was also analyzed by putting aim pollutant + pho tocatalyst solution in dark (for 30 min). About 5 ml sample at regular time interval was withdrawn during the treatment reaction. Centrifugation method has been utilized for separation of photocatalyst from irradiated solution. Absorbance of IMD and MB (0.02 mM) dye solution was recorded at λ = 271 and 663 nm. The % efficacy of each photocatalyst was determined by using below equation:

$$\%removalefficacyoftestedpollutant = [(C_o - C_t)/C_o] \times 100$$

Where C_o symbolizes the initial concentration and C_t designates the concentration after particular irradiation time t of target pollutant.

2.5. Photo-electrochemical test

Bi_2O_3 and Pd@PPC/Bi_2O_3 oriented photocurrent was examined by Zahner CIMPS (PP211) universal photo-electrochemical workstation with Z-photonics accessory. In brief, 3 mg of fabricated nanostructures were dispersed in Nafion (50 μL) + ethanol (450 μL) solution. From this, 1.5 μL solution was carefully put on working electrode in the form of fine smooth layer. During each experiment, Pt and Ag/AgCl wire were positioned as a counter and reference electrode. LED light of 500 Wm^{-2} intensity was used as irradiation source to measure the response of nanostructures employed electrodes under light, the LED light source used is provided in Supplementary Information. All trials were conducted at 0.0 V with 30 s as exposure time to light.

3. Results and discussion

3.1. Structural analysis of Pd@PPC/Bi_2O_3 nanocomposites

XRD investigations were conducted to clarify the crystallinity, purity, and phase of different created samples. Fig. 1 shows the XRD spectral trends of PPC, Bi_2O_3, PPC/Bi_2O_3 and Pd@PPC/Bi_2O_3 samples. XRD pattern of PPC presents a wide, broad peak centered at 2θ = 24.84^0 representing the amorphous structure of PPC and carbon nanocomposite (Daş and Yurtcan, 2016). On the other hand, Bi_2O_3 possesses several distinct peaks at 2θ = 25.82°, 28.11°, 30.23°, 31.8°, 32.87°, 41.49°, 46.35°, 47.16°, 51.27°, 54.51°, 55.59° and 57.83° demonstrating respectively the (210), (201), (211), (002), (220), (212), (222), (400), (123), (203), (421), and (402) planes of the tetragonal arrangement of β-Bi_2O_3 (JCPDS no. 27–0050) (Helal et al., 2016). PPC/Bi_2O_3 composite sample shows XRD peaks of Bi_2O_3, confirming that Bi_2O_3 crystal arrangement remained intact even after the development of hybrid framework with PPC. In PPC/Bi_2O_3 sample, we could not observe any PPC related band, might be due to well-ordered dispersion of polymeric PPC into the Bi_2O_3. Also, in case of Pd@PPC/Bi_2O_3 sample, similar trends like that of PPC/Bi_2O_3 has been achieved with no peak related to Pd NPs which might be due to the lesser Pd content. It is pertinent to mention here that peak intensity has been slightly reduced in case PPC/Bi_2O_3 and Pd@PPC/Bi_2O_3 nanostructures in comparison to Bi_2O_3, indicating proper establishment of hybrid structure amongst the chosen contenders. The XRD results unambiguously reveal the successful fabrication of trio photocatalyst among Bi_2O_3, PPC and Pd. Furthermore, no shift in XRD pattern was observed in case of Pd@PPC/Bi_2O_3 suggesting the impeccable structure of developed photocatalyst. The crystallite size of Bi_2O_3, PPC/Bi_2O_3 and Pd@PPC/Bi_2O_3 samples were also determined using

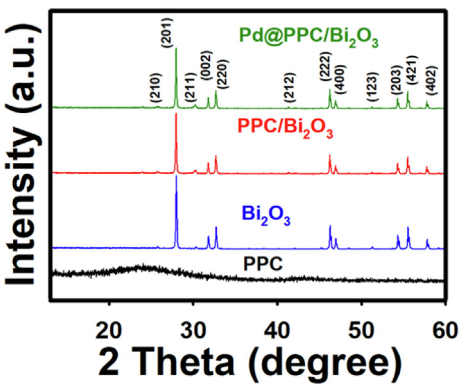

Fig. 1. XRD patterns of PPC, pure Bi_2O_3, PPC/Bi_2O_3, and Pd@PPC/Bi_2O_3 photocatalysts.

the Scherrer's equation (Holder and Schaak, 2019). The crystallite size of pure Bi_2O_3; PPC/Bi_2O_3 and Pd@PPC/Bi_2O_3 samples are 56.01, 55.71 and 54.70 nm, respectively.

FTIR spectra of Bi_2O_3, PPC, PPC/Bi_2O_3 and Pd@PPC/Bi_2O_3 nanocomposites are shown in Fig. 2. The absorption bands at 555 cm^{-1} in Bi_2O_3 as well as in PPC/Bi_2O_3 and Pd@PPC/Bi_2O_3 samples originate due to Bi-O stretching mode (Gurunathan, 2004; Faisal et al., 2014). In case of PPC sample, peaks appeared at 670 and 778 cm^{-1} arise due to C–H plane deformation in polypyrrole (Ahmad et al., 2020) while the peak at 930 cm^{-1} is assigned to doped state of polypyrrole with oxidant (Hayat et al., 2019). Furthermore, two discrete peaks in PPC at 1055 and 1193 cm^{-1} confirmed the = C – H bending and C – N stretching vibrations of polypyrrole (Ahmad et al., 2020). Presence of 670, 930, 1055 and 1194 cm^{-1} peaks of pure PPC in fabricated hybrid samples i.e. PPC/Bi_2O_3 and Pd@PPC/Bi_2O_3, confirmed the effective formation of hybrid photocatalysts among the nominated metabolites.

Diffuse reflectance spectra in UV–visible range have been recorded for Bi_2O_3, PPC, PPC/Bi_2O_3 and Pd@PPC/Bi_2O_3 nanostructures for the evaluation of band gap. It has been observed that photocatalytic performance of any newly created framework exceedingly hinge on its optical features. Revealed spectra for PPC, Bi_2O_3, PPC/Bi_2O_3 and Pd@PPC/Bi_2O_3 nanocomposite are displayed in Fig. 3 (a). Acquired tangent in Kubelka-Munk (K-M) function F(R) *versus* photon-energy plot offered bandgap energy (E_g) for individual photocatalyst as depicted in Fig. 3 (b) for Pd@PPC/Bi_2O_3 photocatalyst. Band gap energies for Bi_2O_3, PPC/Bi_2O_3 and Pd@PPC/Bi_2O_3 nanostructures were found to be 2.55, 2.50 and 2.36 eV, respectively. Attained E_g value for pure Bi_2O_3 is perfectly in line with previous literature (Jiang et al., 2015). The bandgap energy was reduced from 2.55 eV to 2.36 eV for pure material to ternary composite due to the doping of pure metal oxide like Bi_2O_3 with various elements led to creation of new energy levels near the conduction band. The incorporation of elements leads to the distortion of the semiconductor crystal lattice, thus changing its surface characteristics, and led to a decrease in the bandgap (Anna Khlyustova et al., 2020). Encouraging values of bandgap in visible range are fruitful for immense exploitation of developed frameworks under low energy irradiation.

X-ray photoelectron spectroscopy (XPS) was conducted on Pd@PPC/Bi_2O_3 to examine the achieved chemical state of designed trio photocatalyst. Fig. 4(a) exhibited the result of wide scan spectra of created Pd@PPC/Bi_2O_3 photocatalyst. Appearance of Pd, Bi, C, O and N elements in analyzed sample confirmed the perfect establishment of desired trio photocatalyst among preferred metabolites. The narrow scan spectrum of Pd 3d as shown in Fig. 4(b) exhibited two peaks at binding energy 337.73 and 342.82 eV which can be assigned to Pd^{2+} (Shao et al., 2020). Bi 4f XPS spectrum (narrow scan) as displayed in Fig. 4 (c) revealed two peaks marked their presence at binding energies 158.7 and 164.1 eV corroborated respectively to Bi $4f_{7/2}$ and Bi $4f_{5/2}$ spin orbit peaks (Zhang et al., 2016). Fig. 4 (d) shows C1s spectrum of two peaks at binding energies 284.71 and 285.20 eV. The peaks appeared at 284.71 eV and 285.20 eV confirmed sp^2 and sp^3 hybridized carbon atom in the designed photocatalyst, respectively (Sivaranjini et al., 2018; Senthilnathan and Yoshimura, 2017; Dolgov et al., 2015). Fig. 4 (e) exhibited the high-resolution XPS spectra of O1s where the original peak deconvoluted into two peaks at binding energies 530.4 and 531.53 eV. The peak at 530.4 eV signifies the presence of O^{2-} ions, whereas the peak at 531.53 eV corroborated to O^{2-} ions existing in oxygen deficient sites (Faisal et al., 2021). The narrow scan XPS spectrum of N1s as shown in Fig. 4 (f) revealed a single peak at 400.24 eV originated due to [N–(C)3] i.e. nitrogen atom linked to three-carbon atoms (Faisal et al., 2021).

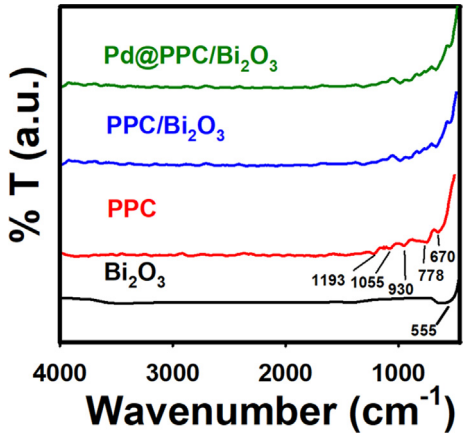

Fig. 2. FTIR examination of Bi_2O_3, PPC, PPC/Bi_2O_3, and Pd@PPC/Bi_2O_3 photocatalysts.

FESEM images in Fig. 5 showed the acquired morphology of scrutinized nanostructures. FESEM image of pure Bi_2O_3 as exhibited in Fig. 5(a) revealed nanoballs like morphology whereas PPC in Fig. 5(b) displayed overlapped layered structures (one layer stacked over another) with layer size 100 to 300 nm. Developed PPC/Bi_2O_3 nanocomposites in Fig. 5(c) have dense layered network of PPC dispersed on Bi_2O_3 nanoballs. Developed ternary photocatalyst has been confirmed in Fig. 5(d) where Bi_2O_3 nanoballs, PPC (layered organizations) and Pd NPs (inside yellow circles) can be easily seen in single frame. EDS examination shown in Fig. 5(e) has also been done on trio framework to assess the elemental compositions. Presence of palladium, bismuth, carbon, oxygen and nitrogen in tested sample further confirmed the existence of ternary framework among Pd, PPC and Bi_2O_3.

TEM images collected in Fig. 6(a–e) were captured to explore the detailed morphology of produced trio framework among Pd, PPC and Bi_2O_3. Pure Bi_2O_3 as presented in Fig. 6 (a) has irregular ball like particles grown abundantly. The size of these nanoballs ranges from 20 to 200 nm while obtained image of PPC as displayed in Fig. 6(b) has stacked layers of dense beads like organization connected well with each other through chain like arrangement. Explored Pd@PPC/ Bi_2O_3 sample as exhibited in Fig. 6(c) revealed a consistently entangled chain of PPC with Bi_2O_3 nanostructures. Efficacious formation of trio photocatalyst among Bi_2O_3, PPC and Pd has been confirmed by the presence of Pd NPs (5–10 nm) in the created organization along with Bi_2O_3 nanostructures and PPC polymeric chains. HRTEM image in Fig. 6 (d) for Bi_2O_3 presented fringe width with 0.28 nm separation, in line with (001) planes of β-Bi_2O_3 (Hou et al., 2013). Furthermore, attained SAED (selected area electron diffraction) trends for Pd@PPC/Bi_2O_3 nanostructures are presented in Fig. 6 (e) demonstrating polycrystalline ring organization clarifying impeccable crystalline structure among selected metabolites.

Acquired Bi_2O_3 and Pd@PPC/Bi_2O_3 nanostructures were also explored for the examination of BET surface area along with total pore volume to check the probable effect of these vital parameters on photocatalytic outcomes of fabricated nanostructures. Both pure as well as hybrid sample were investigated through nitrogen isotherm (adsorption /desorption) technique at 77 K, as presented in Fig. 7. Achieved type IV isotherm in both Bi_2O_3 and Pd@PPC/Bi_2O_3 nanostructures clearly confirmed the mesoporous nature of both materials. Also, both photocatalysts exhibit H4 type hysteresis loop arrangement, enlightening the presence of pores in investigated samples. BET surface areas for Bi_2O_3 and Pd@PPC/Bi_2O_3 nanostructures are observed to be 1.95 and 79.52 m^2/g respectively. It has been clear from attained values that alteration of bare Bi_2O_3 to ternary Pd@PPC/Bi_2O_3 framework boosted up the surface area remarkably to ~ 40.77 times, a clear confirmation of develop-

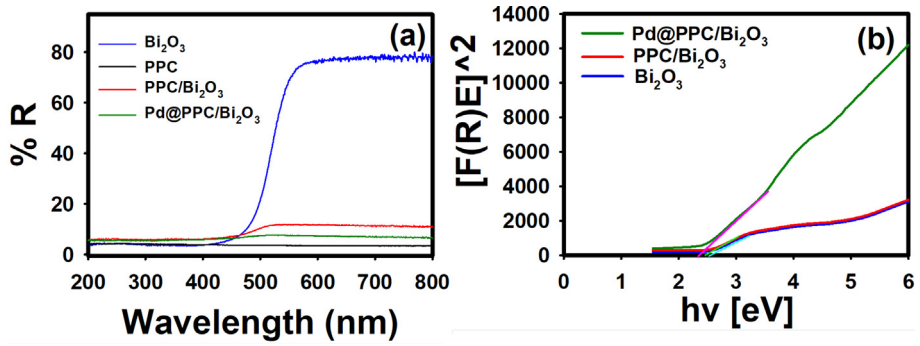

Fig. 3. (a) UV–visible diffuse reflectance spectra of pure Bi_2O_3, PPC, PPC/Bi_2O_3, and Pd@PPC/Bi_2O_3 nanocomposite photocatalysts. (b) The plot of transferred Kubelka–Munk vs. energy of light absorbed for Pd@PPC/Bi_2O_3 photocatalyst.

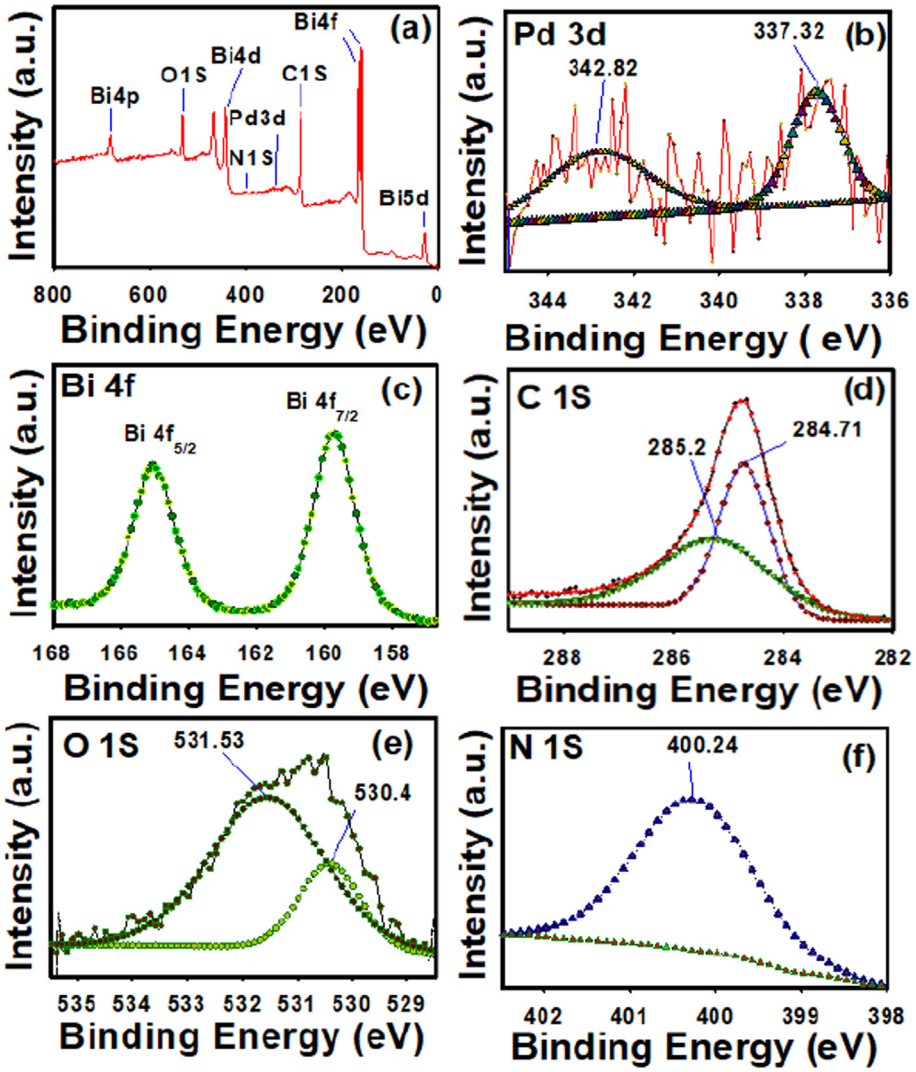

Fig. 4. (a) Wide-scan (survey spectrum) and (b-f) narrow-high resolution scan XPS spectra of Pd@PPC/Bi_2O_3 nanocomposite photocatalyst. The high-resolution scan spectra were recorded respectively for Pd3d, Bi4f, C1s, O1s and N1s.

ment of proficient photocatalyst. Additionally, the pore-size distribution analysis showed 38.50 and 15.3 nm as average pore size for Bi_2O_3 and Pd@PPC/Bi_2O_3, respectively. The BJH adsorption cumulative pore volumes for Bi_2O_3 and Pd@PPC/Bi_2O_3 nanostructures were found to be 0.0188 and 0.3041 cm^3/g, respectively.

3.2. Evaluation of photocatalytic activity

Generation of exceedingly dynamic moieties like $O_2^{\bullet}$ / $^{\bullet}OH$ (Superoxide radical anions or hydroxyl radicals) during photocatalytic reactions is supposed to be the main factor for its dominating

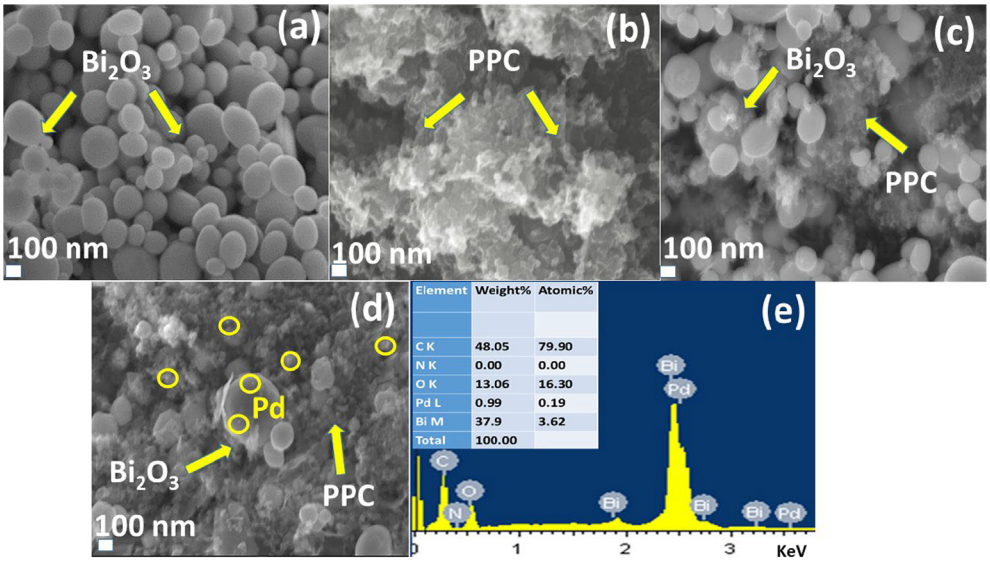

Fig. 5. FESEM images of (a) pure Bi_2O_3 (b) PPC (c) PPC/Bi_2O_3 (d) Pd@PPC/Bi_2O_3 and (e) Energy Dispersive X-ray analysis of Pd@PPC/Bi_2O_3 photocatalyst.

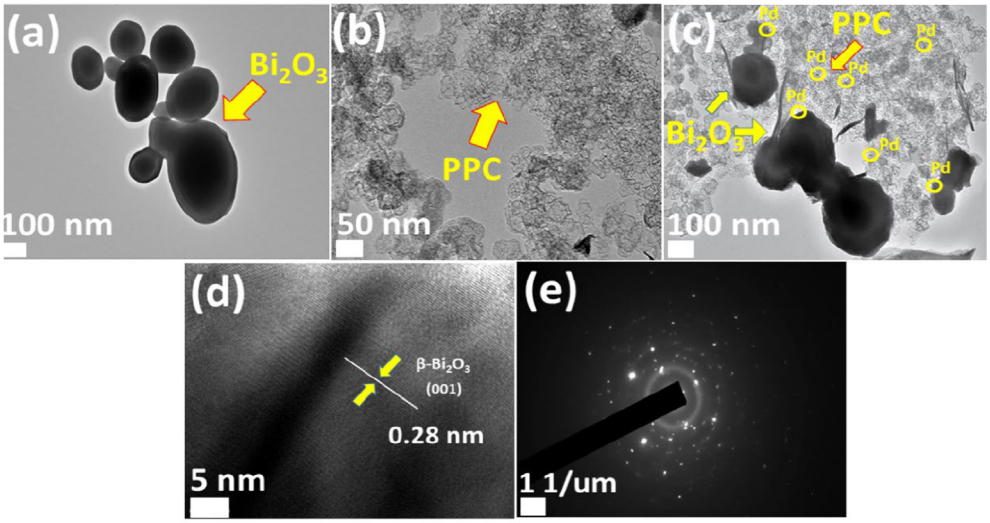

Fig. 6. TEM images of (a) Bi_2O_3 (b) PPC (c) Pd@PPC/Bi_2O_3 (d) HRTEM image of Bi_2O_3 (e) Selected area electron diffraction of Pd@PPC/Bi_2O_3 photocatalyst.

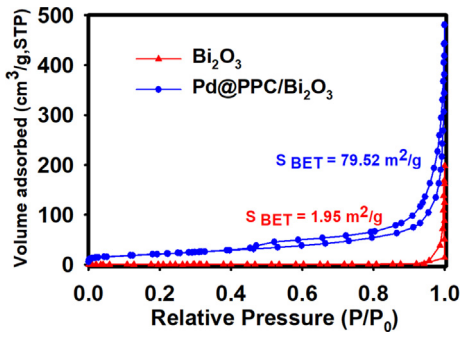

Fig. 7. N_2 sorption isotherm for pure Bi_2O_3 and Pd@PPC/Bi_2O_3 photocatalyst.

nature over the other treatment practices for the efficient destruction of aim pollutants. During the treatment of target analyte, abundantly produced $^{\bullet}OH$ and $O_2^{-\bullet}$ moieties easily led to the breakdown of complicated/rigid structures of hazardous organic pollutants bonded by C–C / C–H or C = C linkage. Another significant requirement for proficient photocatalyst is that the chosen metabolites for the designing of new photocatalytic framework must have adequate surface area with admirable command over separation of charge carriers.

Firstly, the effect of change in pH has been examined on photocatalytic degradation of imidacloprid by changing the solution pH in the range of 4.1 to 10. Solution pH was adjusted by dropwise addition of dilute aqueous solution of either HNO_3 or NaOH. The interpretation of pH impact on photocatalytic reaction is quite complicated task due to its multiple roles such as electrostatic interactions between the photocatalyst surface, solvent molecules, substrate and charged radicals formed during the course of reaction. The ionization state of photocatalyst surface can either be protonated or deprotonated under acidic and alkaline conditions (Abu Tariq et al., 2005). Accomplished degradation rate constant (k) values for the decomposition of target analyte imidacloprid as a function of reaction pH are presented in Fig. S1 (Supplementary Material). As can be seen that degradation rate constant (k) decreases with increase in reaction pH and the highest value was

observed at pH 4.1 i.e. under acidic conditions which might be due to the higher concentration of negatively charged OH^- ions over the catalyst surface at greater pH values, thereby repelling the electron-rich pollutant imidacloprid (Dipyaman Mohanta, 2021; Patil et al., 2014). Obtained results are perfectly in line with previous available reports for imidacloprid degradation (Dipyaman Mohanta, 2021; Patil et al., 2014).

The photodegradation activity of newly accomplished Bi_2O_3, PPC/Bi_2O_3 and Pd@PPC/Bi_2O_3 nanostructures has been effectively assessed on an insecticidal derivative IMD. Aim pollutant was noticed to be fairly stable and steady when treated to bare visible light (i.e., without any photocatalyst) with no observable degradation effect. On the other hand, all fabricated nanostructures of Bi_2O_3, PPC/Bi_2O_3 and Pd@PPC/Bi_2O_3 were reasonably effective for the elimination of IMD. Among different accomplished nanostructures, newly fabricated Pd@PPC/Bi_2O_3 trio photocatalyst was found to be most efficacious with almost complete destruction of IMD molecule after 30 min of irradiation. Fig. S2 displayed the spectra of IMD insecticide after different irradiation times when treated in presence of Pd@PPC/Bi_2O_3 photocatalyst. Obtained spectra of IMD molecule unarguably illuminate the destructing potential of Pd@PPC/Bi_2O_3 photocatalyst. As can be seen the distinctive band of IMD appearing at $\lambda_{max} \sim 271$ nm collapsed entirely after 30 min under Pd@PPC/Bi_2O_3 photocatalyst with shattered absorbance value. These promising outcomes by newly developed Pd@PPC/Bi_2O_3 photocatalyst are in support of its brighter future in environmental management activities.

Removal percentage of IMD molecule with and without different created nanostructures like Bi_2O_3, PPC/Bi_2O_3 and Pd@PPC/Bi_2O_3 is presented in Fig. 8a. It has been clear that under visible light exposure i.e. without photocatalyst no observable degradation of target IMD molecule has been noticed even after 30 min while various tried photocatalysts were noticed to be quite effective on IMD and eliminated the insecticide to various extents. Fabricated hybrid nanostructures exhibited much better performance than bare Bi_2O_3, revealing the prominence of alteration or manipulation during the creation process of novel photocatalytic structures. It has been observed that 60.77 % and 80.87 % of target IMD has been removed under Bi_2O_3 and PPC/Bi_2O_3 nanostructures after 30 min of irradiation. Above all, exceedingly worthwhile degradation of IMD molecule has been occurred under Pd@PPC/Bi_2O_3 photocatalyst with 93.6 % removal of IMD after 30 min, signifying the perfect establishment of efficient photocatalytic structure between Pd NPs, PPC and Bi_2O_3.

Various created nanostructures were also tested for the assessment of k value i.e. photodegradation rate constant which recommends the degradation rate of photocatalyst, as shown in Fig. 8b. Here, the rate constant (k) value of PPC/Bi_2O_3 and Pd@PPC/Bi_2O_3 is much higher than Bi_2O_3, again elucidating the worthiness of composite photocatalyst in environmental cleansing activities. Value of k escalates linearly from 0.0314 min^{-1} to 0.0868 min^{-1} as bare Bi_2O_3 was amended to Pd@PPC/Bi_2O_3 nanocomposite. Achieved highly encouraging rate constant (k) for Pd@PPC/Bi_2O_3 photocatalyst undeniably clarifies the fruitful development of proficient ternary photocatalyst, almost 276 % (~2.76 times) more proficient than Bi_2O_3 and found to be most dominant among all designed nanostructures.

Above experimental studies evidently revealed that PPC/Bi_2O_3 nanostructure is effective than bare Bi_2O_3. Also, precise amendment of PPC/Bi_2O_3 to Pd@PPC/Bi_2O_3 photocatalyst by dispersing Pd nanoparticles led to the creation of most efficacious photocatalyst. Rapid eradication of target IMD by Pd@PPC/Bi_2O_3 photocatalyst might be due to (i) the involvement of polypyrrole with carbon black i.e. PPC in newly established Pd@PPC/Bi_2O_3 nanocomposite. Existing PPC material in nanocomposite makes fluent roaming of electrons towards the conduction band of Bi_2O_3 once excited upon exposure of light. Available electrons acquired surficial part of Bi_2O_3: generate hydroxyl radical ($^{\bullet}OH$) in reaction with water or produce superoxide radical anion ($O_2^{-\bullet}$) once interacted with oxygen. Also, interweaved carbon black in PPC provides hassle free smooth passage for e^-/h^+ pairs for effectual redox reactions. (ii) Developed surface plasmon resonance (SPR) among Pd nanoparticles and Bi_2O_3 enhances the light captivation capabilities of Pd@PPC/Bi_2O_3 nanostructures, ultimately offers admirable photocatalytic performance (Gurunathan, 2004). Besides this, plasmonic effect amongst Pd nanoparticles and Bi_2O_3 also can retard the recombination activity of e^-/h^+ pairs with ample supply of destructive agents like $^{\bullet}OH$ or O_2^- for effective degradation (Zhao et al., 2008; Schmucker et al., 2010; Gaikwad et al., 2018; Hashim et al., 2019). (iii) Presence of Pd NP onto PPC/Bi_2O_3 nanocomposite delivers a photocatalyst (Pd@PPC Bi_2O_3) with lower bandgap as compared to bare Bi_2O_3: a photocatalyst works efficiently well under visible light (iv) Created Pd@PPC/Bi_2O_3 nanocomposite has surface area almost ~ 40.77 times higher than bare Bi_2O_3, another favorable factor responsible for better performance of Pd@PPC/Bi_2O_3 photocatalyst. Therefore, impeccable synergistic coordination among Pd, PPC and Bi_2O_3 is supposed to be the main factors for its excellent photocatalytic activity.

Destructing skills of Pd@PPC/Bi_2O_3 nanostructures have been further verified by employing the created photocatalytic structure for the eradication of complex dye framework i.e. methylene blue (MB). Photocatalytic results in terms of absorbance after different exposure times are displayed in Fig. S3. Adsorption factor was also analyzed by putting MB + photocatalyst solution in dark (for 30 min) since the adsorption capacity of the catalyst plays a crucial role in the photocatalytic performance and it has been observed that 19.5 % of MB has been removed via adsorption onto the photocatalyst. Better is the adsorption skill of any created photocata-

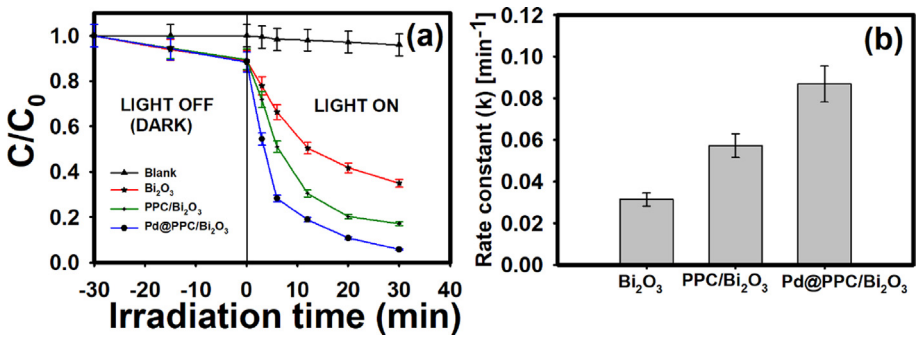

Fig. 8. (a) Change in concentration *versus* irradiation time; and (b) comparison of rate constant (k) for the decomposition of imidacloprid utilizing Bi_2O_3, PPC/Bi_2O_3 and Pd@PPC/Bi_2O_3 photocatalysts.

lyst, encouraging will be its removal efficiency. MB dye molecule exhibited two well distinct humps at 291 and 663 nm. Upon exposure to light in presence of Pd@PPC/Bi_2O_3 nanostructures, both the humps completely lost their identities just in 12 min. It has been observed that absorbance spectral lines became completely flattened just after 12 min verifying the immense striking skills of designed photocatalyst. As per previous studies, it has been suggested that the breakdown or annihilation of MB framework proceeds either via oxidative means or followed two-electron reduction pathway (MB decolorization) with the development of leuco MB (Park and Choi, 2005; Jalalah et al., 2015). During the entire treatment activity, we could not detect any hump or peak signifying the leuco form of MB usually appeared at λ = 256 nm, a clear evidence confirming that the removal of dye followed the oxidative route (Faisal et al., 2021).

The above experiments revealed that eradication of target pollutants significantly enhanced in the presence of Pd@PPC/Bi_2O_3 nanostructures. Hence, it is very important to explore the favorable parameters responsible for pleasing outcomes of Pd@PPC/Bi_2O_3 photocatalyst. For semiconductor photocatalyst, the valence (E_{VB}) and conduction (E_{CB}) band location can be assessed through appended equations (Gaikwad et al., 2018):

$$E_{VB} = \chi - E^e + 0.5E_g$$

$$E_{CB} = E_{VB} - E_g$$

Where χ symbolizes the absolute electronegativity of Bi_2O_3 i.e. 4.686 eV (Devi et al., 2020), E^e represents the energy on hydrogen scale (i.e. 4.5 eV) for free electrons and Eg indicates the bandgap of Bi_2O_3 i.e. 2.50 eV. Utilizing the above the mentioned equations, E_{VB} and E_{CB} for Bi_2O_3 are calculated as 1.44 and −1.06 eV, respectively. Reported value for LUMO and HOMO for PPy is − 1.73 and 0.39 eV vs. NHE, respectively (Liu et al., 2021). Here E_{VB} for Bi_2O_3 is less positive than (OH^-/ $^\bullet OH$) redox potential i.e. ∼ +1.99 eV vs. NHE, so the existing holes at the Bi_2O_3 valence band surface could not oxidize H_2O to deliver $^\bullet OH$ directly. Here, E_{VB} of Bi_2O_3 is more positive than standard oxidation potential of O_2/H_2O i.e. ∼ +1.23 eV vs. NHE (Nwaji et al., 2021), so the holes produced by Bi_2O_3 can react with H_2O to generate hydrogen ions (H^+) and oxygen (O_2). Additionally, the E_{CB} of Bi_2O_3 is well suitable for conversion of O_2 into H_2O_2 (+0.69 eV vs. NHE) (Nwaji et al., 2021). Thus, electrons in conduction band of Bi_2O_3 offered $^\bullet OH$ by multi-electron reaction with oxygen and consume the available O_2 and H^+ ions species. Also, the electrons present at the surface of Bi_2O_3 conduction band (photo-induced electron) can easily transformed the adsorbed O_2 to $O_2^{-\bullet}$ because E_{CB} of Bi_2O_3 is more negative than ($E_{(O_2/O_2^{-\cdot})}$ = -0.046 eV vs. NHE) (Nwaji et al., 2021). These redox reactions produced moieties ($^\bullet OH$ / $O_2^{-\bullet}$) are supposed to be the chief destructive agents for the eradication of noxious contaminants.

A probable photodegradation mechanism in presence of Pd@PPC/Bi_2O_3 for the eradication of IMD is accordingly depicted in Scheme 1. Semiconductors like Bi_2O_3 once illuminated with light energy ≥ band gap energy led to the generation of photo-excited e^-/h^+ pairs, where electrons travel to the conduction band and holes seated in the valence band of Bi_2O_3. Later, these e^- and h^+ travel towards the surface of Bi_2O_3, participate in reaction with available O_2/H_2O to generate dynamic striking agents like $O_2^{-\bullet}$/ $^\bullet$ OH which finally led to the deprivation of target IMD structure. Also, involved polymeric PPC in Pd@PPC/Bi_2O_3 nanostructure can play a significant role. PPC can dynamically offer e^-/h^+ pairs even under visible light exposure. So, PPC exposed to light radiations competently supplies electrons to the conduction band of Bi_2O_3. These electrons then reached to the surficial part of Bi_2O_3: offers hydroxyl radical ($^\bullet$ OH) after reacting with water or offers superoxide radical anion ($O_2^{-\bullet}$) in combination with oxygen, considerably desirable species generated during AOP. Additionally, the occurrence of beneficial plasmonic effect due to the involved Pd NPs improves the separation skill or led to clampdown of ongoing recombination activity with surplus creation of dynamic species like $^\bullet OH$ and $O_2^{-\bullet}$. Overall, the promising synergistic/cumulative effect by Pd NPs, PPC and Bi_2O_3 moieties in Pd@PPC/Bi_2O_3 ternary photocatalyst are supposed the main factor for its excellent results.

The photodegradation products as well as intermediated of insecticidal molecule imidacloprid has been examined/analyzed by several researchers and are well documented in literature (Sharma et al., 2015; Liu et al., 2006). Different structurally related compounds to imidacloprid were observed as possible photodegradation intermediates/products as shown in pathway I, II and III of Scheme 2 (Sharma et al., 2015; Liu et al., 2006). It has been noticed that imidacloprid guanidine and imidacloprid-urea i.e. compound 2 and 3 are most common intermediate forms during the photocatalytic treatment of imidacloprid molecule leading to generation of smaller structures like compound 4, 5 and 6 which can easily degraded to eco- friendly inorganic ions.

Photoluminescence (PL) examination has also been carried out for Bi_2O_3, PPC/Bi_2O_3 and Pd@PPC/Bi_2O_3 nanostructures. The PL spectra as displayed in Fig. 9 (a) have been recorded at 325 nm excitation wavelength. As can be seen, accomplished results in terms of PL spectral intensities followed the order: Bi_2O_3 > PPC/Bi_2O_3 > Pd@PPC/Bi_2O_3 demonstrating that alteration of bare Bi_2O_3 to hybrid nanostructures dropped the PL intensities significantly. Displayed spectra for Pd@PPC/Bi_2O_3 photocatalyst showed spectral hump with lowest intensity among various tested nanostructures, elucidating that the most efficient e^-/h^+ pairs separation has been occurred in Pd@PPC/Bi_2O_3 ternary photocatalyst (Faisal et al., 2018; Ismail et al., 2018). Smooth control over recombination activity by Pd@PPC/Bi_2O_3 photocatalyst is a decisive factor for its efficient and rapid behavior. Our PL investigation is perfectly in line with attained photocatalytic results.

To assess the contribution of each available active species during treatment reaction, several trials were performed in presence of different trapping agents or scavengers. For each test, 0.01 M of scavenger i.e. potassium iodide (KI) for hole (h^+), ascorbic acid (AA) for superoxide radical anion ($O_2^{-\bullet}$) and isopropyl alcohol (IPA) for hydroxyl radicals ($^\bullet OH$) scavenging moiety were taken with Pd@PPC/Bi_2O_3 photocatalyst in MB solution (Faisal et al., 2021; Helal et al., 2017). As revealed from Fig. 9 (b), photodegradation activity under IPA was retarded severely, confirming that the produced hydroxyl radicals ($^\bullet OH$) are the prime destructive candidate during photocatalytic treatment of pollutant. In addition to this, presence AA and KI along with photocatalyst also retards the degradation rate to some degree, demonstrating that $O_2^{-\bullet}$ as well as h^+ have supportive effect during the treatment reaction along with main destructive candidate i.e. hydroxyl radicals.

Trials were also performed to determine the electrochemically generated photocurrent by Bi_2O_3 and Pd@PPC/Bi_2O_3 nanostructures and particular responses are displayed in Fig. 10. Incessant movement of charge from Bi_2O_3 or Pd@PPC/Bi_2O_3 nanostructures to outer circuit led to the photocurrent generation, superior is the charge separation encouraging will be the obtained photocurrent response through nanostructures (Faisal et al., 2022). Photocurrent response increases considerably as bare Bi_2O_3 was manipulated to Pd@PPC/Bi_2O_3 nanocomposites. Pleasing and acknowledgeable response in case of Pd@PPC/ Bi_2O_3 might be due to efficacious decline in e^-/h^+ pairs recombination with prompt electrons flow towards the surface of semiconductor. Accomplished electrochemically generated photocurrent is in line to our tested photocatalytic results.

Stability and reusability are two major concerns regarding the practical implementation of any newly generated photocatalyst.

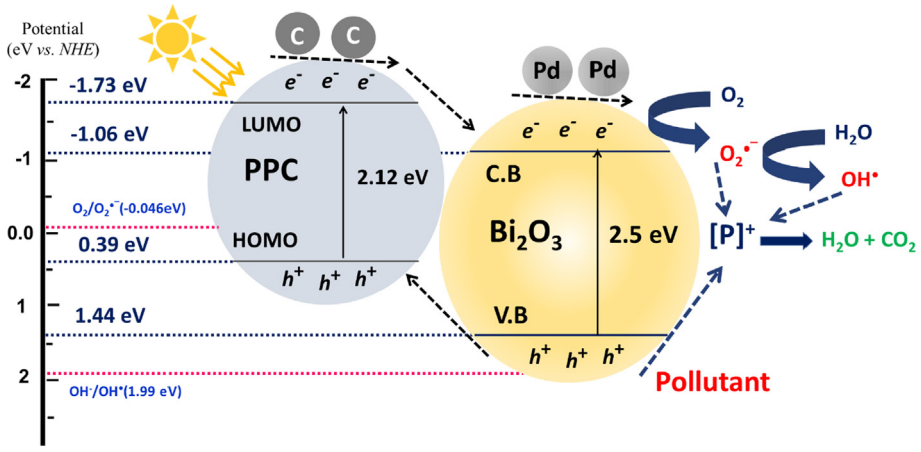

Scheme 1. Proposed schematic representation during the photodegradation and charge transfer at the surface of Pd@PPC/Bi_2O_3 nanocomposite photocatalyst.

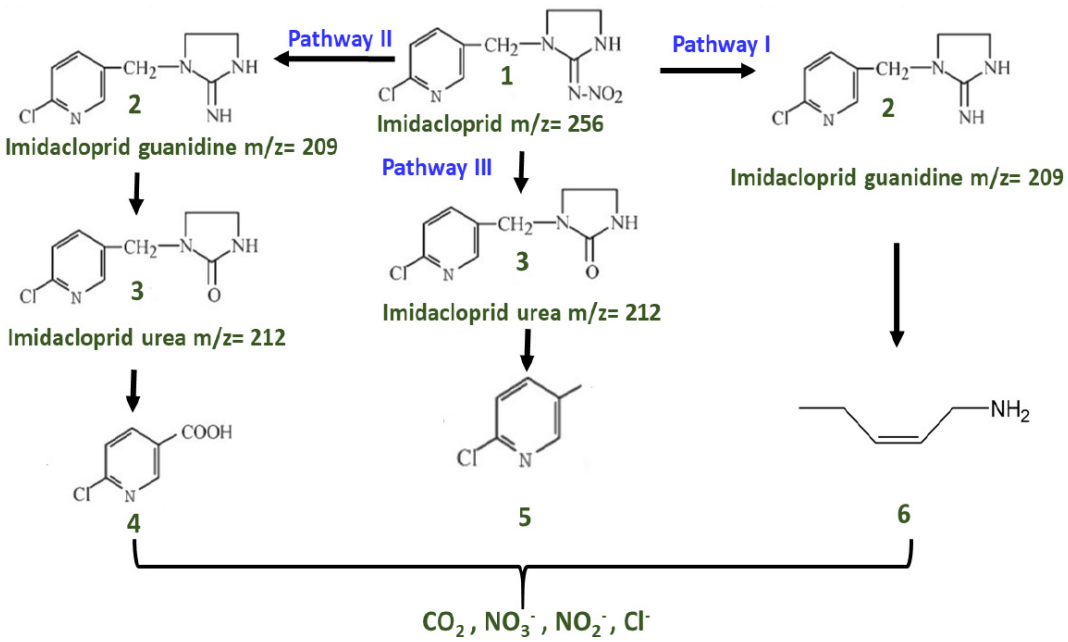

Scheme 2. Proposed pathway for the degradation of imidacloprid.

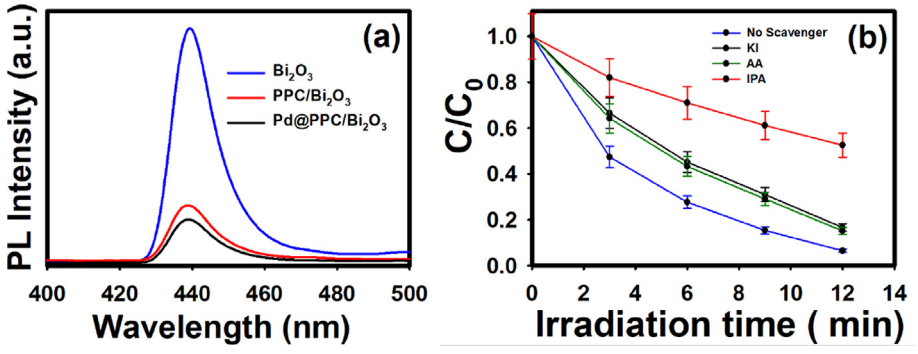

Fig. 9. (a) Photoluminescence (PL) spectra of Bi_2O_3, PPC/Bi_2O_3 and Pd@PPC/Bi_2O_3 nanocomposites (excited at λ = 325 nm). (b) Reactive species scavenging experiments on MB dye using Pd@PPC/ Bi_2O_3 photocatalyst in the presence of different scavenging moieties.

So, among various created photocatalysts, most potent Pd@PPC/ Bi_2O_3 has been tested for the elimination of MB for five continuous photocatalytic runs and their results are displayed in Fig. 11. Newly accomplished Pd@PPC/Bi_2O_3 photocatalyst was observed to be sufficiently stable even after five consecutive trials with almost negligible deterioration in % removal efficacy.

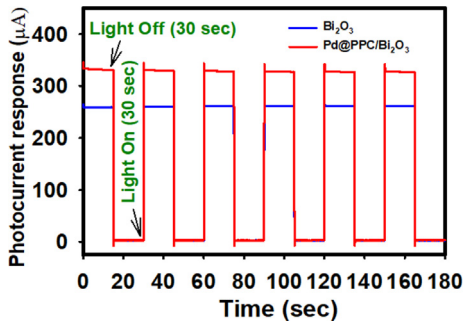

Fig. 10. Photocurrent behavior (photocurrent vs. time) measured for Bi_2O_3 and Pd@PPC/Bi_2O_3 nanocomposite at 0.0 V applied potential, light exposure time = 30 s, lamp intensity = 500 Wm^{-2}.

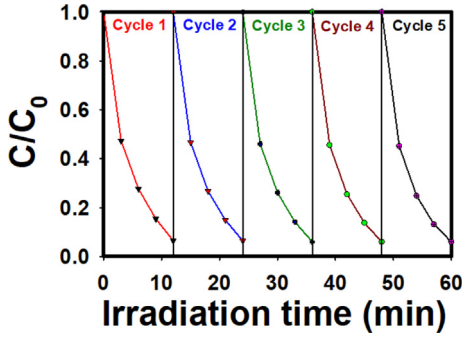

Fig. 11. Repeated tests up to 5 times for the photocatalytic degradation of MB in presence of Pd@PPC/Bi_2O_3 photocatalyst.

Exceedingly steady results could be decidedly noteworthy as far as the future/practical execution of tried photocatalyst is concern. During the washing/extraction procedure after each trail, there might be loss of some active material which in turn may be the reason behind the slight dropping in photocatalytic activity.

Furthermore, XRD results of tested Pd@PPC/Bi_2O_3 before and after cyclic tests demonstrate that there was no deterioration in the arrangement of designed photocatalyst. Fig. S4 (a) exhibits that the crystallinity and configuration of the created nanohybrid remain preserved even after five cyclic experiments. Furthermore, FESEM image of tested photocatalyst Pd@PPC/Bi_2O_3 after cyclic experiments clearly suggests that the morphology of developed ternary nanocomposite preserved even after several trials as shown in Fig. S4 (b).

4. Conclusions

Novel Pd@PPC/Bi_2O_3 ternary nanocomposite photocatalyst has been created utilizing simple, reliable, cost-effective, and stress-free ultra-sonication approach followed by photo-reduction technique. Created Pd@PPC/Bi_2O_3 ternary photocatalyst exhibited promising photodegradation activity on insecticide IMD as compared with bare Bi_2O_3 photocatalyst. Pd@PPC/Bi_2O_3 exhibited excellent photodegradation performance with 93.6 % removal of insecticide IMD just in 30 min. Also, the Pd@PPC/Bi_2O_3 photocatalyst was found to be remarkably well for the destruction of MB with complete removal of rigid dye molecule in 12 min. Synergistic effects by Pd NPs, PPC and Bi_2O_3 in designed ternary structure offered encouraging charge-separation with swift flow of charge carriers resulting in efficient photodegradation activity. Promising and steady outcomes by Pd@PPC/Bi_2O_3 nanostructures are highly vital features for its brighter future in environmental remediation related fields.

Declaration of competing interest

The authors declare that they have no known competing financial interests or personal relationships that could have appeared to influence the work reported in this paper.

Acknowledgements

Authors would like to acknowledge the support of the Deputyship for Research and Innovation-Ministry of Education, Kingdom of Saudi Arabia for this research through a grant (NU/IFC/2/SERC/-/18) under the Institutional Funding Committee at Najran University, Kingdom of Saudi Arabia.

Appendix A. Supplementary material

Supplementary data to this article can be found online at https://doi.org/10.1016/j.arabjc.2023.105349.

References

M. Abu Tariq, M. Faisal, M. Muneer, Semiconductor-mediated photocatalysed degradation of two selected azo dye derivatives, amaranth and bismarck brown in aqueous suspension, J. Hazard. Mater. B127 (2005) 172.
Ahmad, S., Khan, I., Husain, A., Khan, A., Asiri, A.M., 2020. Electrical conductivity based ammonia sensing properties of polypyrrole/MoS_2 nanocomposite. Polymers 12, 3047.
Alam, U., Fleisch, M., Kretschmer, I., Bahnemann, D., Muneer, M., 2017. One-step hydrothermal synthesis of Bi-TiO_2 nanotube/graphene composites: An efficient photocatalyst for spectacular degradation of organic pollutants under visible light irradiation. Appl. Catal. B: Environ. 218, 758.
Anandan, S., Lee, G.-J., Chen, P.-K., Fan, C., Wu, J.J., 2010. Removal of Orange II dye in water by visible light assisted photocatalytic ozonation using Bi_2O_3 and Au/Bi_2O_3 nanorods. Ind. Eng. Chem. Res. 49, 9729.
Doped TiO_2: the effect of doping elements on photocatalytic activity , Anna Khlyustova, Nikolay Sirotkin, Tatiana Kusova, Anton Kraev, Valery Titov and Alexander Agafonov, Material Advance 1 (2020) 1193.
Ansari, R., 2006. Polypyrrole conducting electroactive polymers: synthesis and stability studies. J. Chem. 3 (4), 186.
Costi, R., Saunders, A.E., Elmalem, E., Salant, A., Banin, U., 2008. Visible light-induced charge retention and photocatalysis with hybrid CdSe-Au nanodumbbells. Nano Lett. 8, 637.
Costi, R., Cohen, G., Salant, A., Rabani, E., Banin, U., 2009. Electrostatic force microscopy study of single Au– CdSe hybrid nanodumb bells: Evidence for light-induced charge separation. Nano Lett. 9, 2031.
Daniel, M.-C., Astruc, D., 2004. Gold nanoparticles: assembly, supramolecular chemistry, quantum-size-related properties, and applications toward biology, catalysis, and nanotechnology. Chem. Rev. 104, 293.
Daş, E., Yurtcan, A.B., 2016. Effect of carbon ratio in the polypyrrole/carbon composite catalyst support on PEM fuel cell performance. Int. J. Hydrogen Energy 41, 13171.
Devi, K.R.S., Mathew, S., Rajan, R., Georgekutty, J., Pinheiro, D., Ananthapadmanabhan, U., Sundararajan, M., 2020. Synthesis and characterization of $CeO_2/Bi_2O_3/gC_3N_4$ ternary Z-scheme nanocomposite. Int. J. Appl. Ceram. Technol. 17, 2346.
Dipyaman Mohanta, Md. Ahmaruzzaman, Au–SnO_2–CdS ternary nanoheterojunction composite for enhanced visible light-induced photodegradation of imidacloprid, Environ. Res. 201 (2021) 111586.
Dolgov, A., Lopaev, D., Lee, C.J., Zoethout, E., Medvedev, V., Yakushev, O., Bijkerk, F., 2015. Characterization of carbon contamination under ion and hot atom bombardment in a tin-plasma extreme ultraviolet light source. Appl. Surf. Sci. 353, 708.
Drache, M., Roussel, P., Wignacourt, J.P., 2007. Structures and oxide mobility in Bi-Ln-O materials: heritage of Bi_2O_3. Chem. Rev. 107, 80.
Elmalem, E., Saunders, A.E., Costi, R., Salant, A., Banin, U., 2008. Growth of photocatalytic CdSe–Pt nanorods and nanonets. Adv. Mater. 20, 4312.
M. Faisal, S.B. Khan, M.M. Rahman, A. Jamal, Abdullah M. Asiri, M.M. Abdullah, Synthesis, characterizations, photocatalytic and sensing studies of ZnO nanocapsules, Appl. Surf. Sci. 258 (2011) 672.
M. Faisal, F. A. Harraz, A. A. Ismail, A. Mohamed El-Toni, S.A. Al-Sayari, A. Al-Hajry, M.S. Al-Assiri, Polythiophene/mesoporous $SrTiO_3$ nanocomposites with enhanced photocatalytic activity under visible light, Sep. Purif. Technol.190 (2018) 33.
Faisal, M., Khan, S.B., Rahman, M.M., Jamal, A., Asiri, A.M., Abdullah, M.M., 2011. Smart chemical sensor and active photo-catalyst for environmental pollutants. Chem. Eng. J. 173, 178.
Faisal, M., Ibrahim, A.A., Bouzid, H., Al-Sayari, S.A., Al-Assiri, M.S., Ismail, A.A., 2014. Hydrothermal synthesis of Sr-doped α-Bi_2O_3 nanosheets as highly efficient photocatalysts under visible light. J. Mol. Catal. A. Chem. 387, 69.

Faisal, M., Jalalah, M., Harraz, F.A., El-Toni, A.M., Labis, J.P., Al-Assiri, M.S., 2021. A novel Ag/PANI/$ZnTiO_3$ ternary nanocomposite as a highly efficient visible-light-driven photocatalyst. Sep. Purif. Technol. 256, 117847.

Faisal, M., Rashed, M.A., Alhmami, M.A.M., Harraz, F.A., 2021. Clean light oriented ultrafast Pt/Bi_2S_3 nanoflakes for the photocatalytic destruction of gemifloxacin mesylate drug and methylene blue. J. Photochem. Photobiol. A Chem. 414, 113288.

Faisal, M., Rashed, M.A., Ahmed, J., Alsaiari, M., Alkorbi, A.S., Jalalah, M., Alsareii, S.A., Harraz, F.A., 2021. Rapid photodegradation of linezolid antibiotic and methylene blue dye over Pt nanoparticles/polypyrrole-carbon black/ZnO novel visible light photocatalyst. J. Environ. Chem. Eng. 9, 106773.

Faisal, M., Rashed, M.A., Ahmed, J., Alhmami, M.A.M., Asif Khan, M.K., Jalalah, M., Alsareii, S.A., Harraz, F.A., 2022. Pt nanoparticles decorated chitosan/$ZnTiO_3$: Ternary visible-light photocatalyst for ultrafast treatment of insecticide imidacloprid and methylene blue. J. Taiwan Inst. Chem. Eng. 133, 104266.

Farah, M.A., Ateeq, B., Ali, M.N., Sabir, R., Ahmad, W., 2004. Studies on lethal concentrations and toxicity stress of some xenobiotics on aquatic organisms. Chemosphere 55, 257.

Figuerola, A., van Huis, M., Zanella, M., Genovese, A., Marras, S., Falqui, A., Zandbergen, H.W., Cingolani, R., Manna, L., 2010. Epitaxial CdSe Au nanocrystal heterostructures by thermal annealing. Nano Lett. 10, 3028.

Gade, R., Ahemed, J., Yanapu, K.L., Abate, S.Y., Tao, Y.-T., Pola, S., 2018. Photodegradation of organic dyes and industrial wastewater in the presence of layer-type perovskite materials under visible light irradiation. J. Environ. Chem. Eng. 6, 4504.

R. Gade, M. Basude, N. B. Simhachalam, R. Devi V, S. Pola , P. Chetti, Synthesis of titanates for photomineralization of industrial wastewater and organic pollutants , Environ. Sci.: Water Res. Technol., 8 (2022) 3065-3078.

P. Gaikwad , C.A. Betty , Jagannath , A. Kumar , R. Sasikala , Microflowers of Pd doped ZnS for visible light photocatalytic and photoelectrochemical applications , Materials Science in Semiconductor Processing 86 (2018) 139.

Gurunathan, K., 2004. Photocatalytic hydrogen production using transition metal ions-doped γ Bi2O3 semiconductor particles Int. J. Hydrogen Energy 29, 933.

Haldar, K.K., Sinha, G., Lahtinen, J., Patra, A., 2012. Hybrid colloidal Au-CdSe pentapod heterostructures synthesis and their photocatalytic properties. ACS Appl. Mater. Interfaces 4, 6266.

Hashim, F.S., Alkaim, A.F., Salim, S.J., Alkhayatt, A.H.O., 2019. Effect of (Ag, Pd) doping on structural, and optical properties of ZnO nanoparticales: As a model of photocatalytic activity for water pollution treatment. Chem. Phys. Lett. 737, 136828.

Hayat, A., Raziq, F., Khan, M., Ullah, I., Rahman, M.U., Khan, W.U., Khane, J., Ahmad, A., 2019. Visible-light enhanced photocatalytic performance of polypyrrole/g-C_3N_4 composites for water splitting to evolve H_2 and pollutants degradation. J. Photochem. Photobiol. A Chem. 379, 88.

Helal, A., Ahamed, M., Akhtar, M.J., Khan, M.A.M., Alaizeri, Z.M., Alhadlaq, H., 2016. Facile synthesis of Zn-doped Bi_2O_3 nanoparticles and their selective cytotoxicity toward cancer cells. ACS Omega 6, 17353.

Helal, A., Harraz, F.A., Ismail, A.A., Sami, T.M., Ibrahim, I.A., 2017. Hydrothermal synthesis of novel heterostructured Fe_2O_3/Bi_2S_3 nanorods with enhanced photocatalytic activity under visible light. Appl. Catal. B Environ. 213, 18.

Ho, C.H., Chan, C.H., Huang, Y.S., Tien, L.C., Chao, L.C., 2013. The study of optical band edge property of bismuth oxide nanowires α-Bi_2O_3. Opt. Express 21, 11965.

Holder, C.F., Schaak, R.E., 2019. Tutorial on powder X-ray diffraction for characterizing nanoscale materials. ACS Nano 13, 7359.

J. Hou, C. Yang, Z. Wang, W. Zhou, S. Jiao, H. Zhu, In situ synthesis of α-βphase heterojunction on Bi_2O_3 nanowires with exceptional visible-light photocatalytic performance, Appl. Catal., B 142–143 (2013) 504.

Huang, Y., Tao, J., Meng, W., Zhu, M., Huang, Y., Fu, Y., Gao, Y., Zhi, C., 2015. Super-high rate stretchable polypyrrole-based supercapacitors with excellent cycling stability. Nano Energy 11, 518.

Ismail, A.A., Faisal, M., Al-Haddad, A., 2018. Mesoporous WO_3-graphene photocatalyst for photocatalytic degradation of MB dye under visible light illumination. J. Environ. Sci. 66, 328.

Jakob, M., Levanon, H., Kamat, P.V., 2003. Charge Distribution between UV-Irradiated TiO2 and Gold Nanoparticles: Determination of Shift in the Fermi Level. Nano Lett. 3, 353.

Jalalah, M., Faisal, M., Bouzid, H., Park, J.-G., Al-Sayari, S.A., Ismail, A.A., 2015. Comparative study on photocatalytic performances of crystalline α- and β-Bi_2O_3 nanoparticles under visible-light. J. Ind. Eng. Chem. 30, 183.

Jeon, S., Moon, J.M., Lee, E.S., Kim, Y.H., Cho, Y., 2014. An electroactive biotin-doped polypyrrole substrate that immobilizes and releases EpCAM-positive cancer cells. Angew. Chem. Int. Ed. 126, 4685.

Jiang, H.-Y., Li, P., liu, G., Ye, J., Lin, J., 2015. Synthesis and photocatalytic properties of metastable β-Bi 2 O 3 stabilized by surface-coordination effects. J. Mater. Chem. A 3, 5119.

Larkin, I.A., Stockman, M.I., Achermann, M., Klimov, V.I., 2004. Dipolar emitters at nanoscale proximity of metal surfaces: Giant enhancement of relaxation in microscopic theory. Phys. Rev. B 69, 121403.

Leontie, L., Caraman, M., Alexe, M., Harnagea, C., 2002. Structural and optical characteristics of bismuth oxide thin films. Surf. Sci. 507–510, 480.

Li, X., Wu, D., Luo, Q., Wang, D., 2017. Advanced cyclized polyacrylonitrile (CPAN)/CdS nanocomposites for highly efficient visible-light photocatalysis. J. Mater. Sci. 52, 736.

Li, X., Wu, D., Luo, Q., Wang, D., 2017. Fabrication of CPAN/Ag/AgCl composites and their efficient visible-light photocatalytic activity. J. Alloy. Compd. 702, 585.

Li, Y., Zhang, Z., Zhang, Y., Sun, X., Zhang, J., Wang, C., Peng, Z., Si, H., 2014. Preparation of Ag doped Bi2O3 nanosheets with highly enhanced visible light photocatalytic performances. Ceram. Int. 40, 13275.

Lin, S.E., Wei, W.C.J., 2011. Long-term degradation of Ta_2O_5-doped Bi_2O_3 systems. J. Eur. Ceram. Soc. 31, 3081.

S. Liu, X. Jiang, G.I.N. Waterhouse, Z.-M. Zhang, L.-min Yu, Protonated graphitic carbon nitride/polypyrrole/reduced graphene oxide composites as efficient visible light driven photocatalysts for dye degradation and E. coli disinfection, Journal of Alloys and Compounds 873 (2021) 159750.

Liu, W., Zheng, W., Ma, Y., Liu, K.K., 2006. Sorption and degradation of imidacloprid in soil and water. J. Environ. Sci. Health B 41, 623.

Luo, Q., Yang, X., Wang, D., 2017. Facile preparation of well-dispersed ZnO/cyclized polyacrylonitrile nanocomposites with highly enhanced visible-light photocatalytic activity. Appl. Catal. B 204, 304.

Lv, S., Du, Y., Wu, F., Cai, Y., Zhou, T., 2022. Review on LSPR assisted photocatalysis: effects of physical fields and opportunities in multifield decoupling. Nanoscale Adv. 4, 2608–12263.

Marschall, R., Wang, L., 2014. Non-metal doping of transition metal oxides for visible-light photocatalysis. Catal. Today 225, 111.

Masula, K., Bhongiri, Y., Rao, G.R., Kumar, P.V., Pola, S., Basude, M., 2022. Evolution of photocatalytic activity of CeO_2–Bi_2O_3 composite material for wastewater degradation under visible-light irradiation. Opt. Mater. 126, 112201.

K. Masula, P. Sreedhar, P. Vijay Kumar, Y. Bhongiri, S. Pola, M. Basude, Synthesis and characterization of NiO–Bi_2O_3 nanocomposite material for effective photodegradation of the dyes and agricultural soil pollutants, Mater. Sci. Semicond. Process.160 (2023) 107432.

Mehring, M., 2007. From molecules to bismuth oxide-based materials: Potential homo-and heterometallic precursors and model compounds. Coord. Chem. Rev. 251, 974.

Naficy, S., Stoboi, N., Whitten, P.G., Spinks, G.M., Wallace, G.G., 2013. Evaluation of encapsulating coatings on the performance of polypyrrole actuators. Smart Mater. Struct. 22, 075005.

M.F. Nsib, N. Naffati, A. Rayes, N. Moussa, A. Houas, A. Effect of some operational parameters on the hydrogen generation efficiency of Ni-ZnO/PANI composite under visible-light irradiationMater. Res. Bull. 70 (2015) 530.

Nwaji, N., Akinoglu, E.M., Giersig, M., 2021. Gold nanoparticle-decorated Bi_2S_3 nanorods and nanoflowers for photocatalytic wastewater treatment. Catalysts 11, 355.

Oh, S.-W., Rhee, H.W., Lee, C., Kim, Y.C., Kim, J.K., Yu, J.-W., 2005. The photovoltaic effect of the p–n heterojunction organic photovoltaic device using a nano template method. Curr. Appl. Phys. 5 (1), 55.

Pan, A., Ghosh, A., 2000. A new family of lead–bismuthate glass with a large transmitting window. J. Non Cryst. Solids 271, 157.

Park, H., Choi, W., 2005. Photocatalytic reactivities of Nafion-coated TiO_2 for the degradation of charged organic compounds under UV or visible -light. J. Phys. Chem. B 109, 11667.

L.T. Parvathi, M. Arunpandian, S. Arunachalam, S. Karuthapandian Visible-light-driven Pd doped β-Bi_2O_3 nanocomposite: an affordable and an efficient catalyst for mitigation of noxious pollutant. Appl. Phys. A 127(2021)535.

Patil, P.N., Bote, S.D., Gogate, P.R., 2014. Degradation of imidacloprid using combined advanced oxidation processes based on hydrodynamic cavitation. Ultrason. Sonochem. 21, 1770–1777.

M.A. Pérez, M.L. Teijelo, Cathodic behavior of bismuth. I. Ellipsometric study of the electroreduction of thin Bi_2O_3 films, J. Electroanal. Chem. 583 (2005) 212.

V. Rao D., M. Subburu, R. Gade, M. Basude, P. Chetti, N. B. Simhachalam , P. Nagababu, Y. Bhongiri, S. Pola, A new Zn (II) complex-composite material: piezo-enhanced photomineralization of organic pollutants and wastewater from the lubricant industry, Environ. Sci.: Water Res. Technol., 7 (2021)1737-1747.

Riaz, U., Ashraf, S.M., Kashyap, J., 2015. Enhancement of photocatalytic properties of transitional metal oxides using conducting polymers: A mini review. Mater. Res. Bull. 71, 75.

Sagarzazu, G., Inoue, K., Saruyama, M., Sakamoto, M., Teranishi, T., Masuo, S., Tamai, N., 2013. Ultrafast dynamics and single particle spectroscopy of Au–CdSe nanorods. PCCP 15, 2141.

Sarat, S., Sammes, N., Smirnova, A., 2006. Bismuth oxide doped scandia-stabilized zirconia electrolyte for the intermediate temperature solid oxide fuel cells. J. Power Sources 160, 892.

Schmucker, A.L., Harris, N., Banholzer, M.J., Blaber, M.G., Osberg, K.D., Schatz, G.C., Mirkin, C.A., 2010. Correlating nanorod structure with experimentally measured and theoretically predicted surface plasmon resonance. ACS Nano 4, 5453.

Senthilnathan, J., Yoshimura, M., 2017. Low energy liquid plasma for direct reduction and formation of rGO-aminopyridine hybrid for electrical and environmental applications. J. Hazard. Mater. 340, 26.

Shao, X., Miao, X., Yu, X., Wang, W., Ji, X., 2020. Efficient synthesis of highly dispersed ultrafine Pd nanoparticles on a porous organic polymer for hydrogenation of CO_2 to formate. RSC Adv. 10, 9414.

Sharma, T., Toor, A.P., Rajor, A., 2015. Photocatalytic degradation of imidacloprid in soil: Application of response surface methodology for optimization of parameters. RSC Adv. 5, 25059.

Shaviv, E., Schubert, O., Alves-Santos, M., Goldoni, G., Di Felice, R., Valle, F., Del Fatti, N., Banin, U., Sçnnichsen, C., 2011. Absorption properties of metal-semiconductor hybrid nanoparticles. ACS Nano 5, 4712.

Shi, Y., Pan, L., Liu, B., Wang, Y., Cui, Y., Bao, Z., Yu, G., 2014. Nanostructured conductive polypyrrole hydrogels as high-performance, flexible supercapacitor electrodes. J. Mater. Chem. A 2, 6086.
Shimanoe, K., Suetsugu, M., Miura, N., Yamazoe, N., 1998. Bismuth oxide thin film as new electrochromic material. Solid State Ion. 113–115, 415.
Shimizugawa, Y., Sugimoto, N., Hirao, K., 1997. X-ray absorption fine structure glasses containing Bi2O3 with third-order non-linearities. J. Non Cryst. Solids 221, 208.
Sivaranjini, B., Mangaiyarkarasi, R., Ganesh, V., Umadevi, S., 2018. Vertical alignment of liquid crystals over a functionalized flexible substrate. Sci. Rep. 8, 8891.
M. Vila, C. Díaz-Guerra, J. Piqueras, Luminescence and Raman study of α-Bi_2O_3 ceramics, Mater. Chem. Phys. 133 (2012) 559.
Yao, T., Cui, T., Wang, H., Xu, L., Cui, F., Wu, J., 2014. A simple way to prepare Au@ polypyrrole/Fe_3O_4 hollow capsules with high stability and their application in catalytic reduction of methylene blue dye. Nanoscale 6, 7666.
Yilmaz, S., Turkoglu, O., Ari, M., Belenli, I., 2011. Electrical conductivity of the ionic conductor tetragonal (Bi2O3)1–x(Eu2O3)x. Cerâmica 57, 185.
Zha, Z., Yue, X., Ren, Q., Dai, Z., 2013. Uniform polypyrrole nanoparticles with high photothermal conversion efficiency for photothermal ablation of cancer cells. Adv. Mater. 25, 777.
Zhang, X., Wang, C.Y., Wang, L.W., Huang, G.X., Wang, W.K., Yu, H.Q., 2016. Fabrication of $BiOBr_xI_{1-x}$ photocatalysts with tunable visible light catalytic activity by modulating band structures. Sci. Rep. 6, 22800.
Zhao, J., Pinchuk, A.O., Mcmahon, M.J., Li, S., Ausman, L.K., Atkinson, A.L., Schatz, G. C., 2008. Methods for describing the electromagnetic properties of silver and gold nanoparticles. Acc. Chem. Res. 41, 1710.
Zhong, J., Li, J., Feng, F., Fan, G., Zeng, J., Huang, S., Hu, W., Li, M., 2014. Improved photocatalytic decolorization of methyl orang over Pd-doped Bi_2O_3. Environ. Prog. Sustain. Energy 33, 1229.